Formation and structure of ZIF-8@PEO coating on the surface of zinc

V. Kasneryk[1*], M. P. M. Poschmann[2], M. Serdechnova[1], G. Dovzhenko[3], D. C. F. Wieland[4], P. Karlova[1], T. Naacke[1], M. Starykevich[5], C. Blawert[1], N. Stock[2,6], M.L. Zheludkevich[1,7]

[1]Institute of Surface Science, Helmholtz-Zentrum Hereon, Max-Planck-Straße 1, 21502 Geesthacht, Germany

[2]Institute of Inorganic Chemistry, CAU Kiel University, Max-Eyth-Straße 2, D-24118 Kiel, Germany

[3]Institute of Materials Physics, Helmholtz-Zentrum Hereon, Max-Planck Strasse 1, 21502 Geesthacht, Germany

[4]Institute of Metallic Biomaterials, Helmholtz-Zentrum Hereon, Max-Planck Strasse 1, 21502 Geesthacht, Germany

[5]Department of Materials and Ceramic Engineering, CICECO - Aveiro Institute of Materials, University of Aveiro, 3810-193 Aveiro, Portugal

[6]Kiel Nano, Surface and Interface Science (KiNSIS)

[7]Faculty of Engineering, CAU Kiel University, Kaiserstrasse 2, 24143 Kiel, Germany

Highlights

- ZIF-8@PEO coating was obtained by transformation of PEO layers with 2-methylimidazole.
- ZIF-8@PEO coating with different distribution of ZIF-8 through PEO can be prepared.
- The multi-stage mechanism of PEO layer into ZIF-8@PEO coating was proposed.

Abstract

Recently, plasma electrolytic oxidation (PEO) found broad application as a multi-purpose process to create effective corrosion and wear resistant coatings on various metallic substrates. The exceptional properties of metal organic frameworks (MOFs) put them also in focus as perspective materials for corrosion protection. In this work, the formation of a novel ZIF-8@PEO coating is reported for the first time. It was synthesized by controllable recrystallization of a PEO layer formed on zinc alloy Z1 into ZIF-8 in the presence of 2-methylimidazole organic linkers. The

multi-stage mechanism of PEO to ZIF-8 rearrangement is proposed. Cross section, glow discharge optical emission spectroscopy and nano-focused synchrotron X-ray diffraction demonstrated that varying of synthesis parameters, the ZIF-8@PEO coating with different distribution of ZIF-8 through PEO layer can be prepared. Based on the results of laser scanning microscopy, the surface smoothing was observed with increasing the degree of the PEO-to-ZIF-8 rearrangement. Containing two components, the novel ZIF-8@PEO coating is expected to combine admirable physical-chemical properties of both PEO and ZIF-8. Such a feature can open the way for its potential application not only for corrosion protection, but also for photo- and heterogeneous catalysis.

Key words: plasma electrolytic oxidation, metal organic frameworks, zeolitic-imidazolate framework, multifunctional coating

1. Introduction

Recently, plasma electrolytic oxidation (PEO) was widely disseminated as a multi-purpose approach to create multifunctional coatings on different metallic substrates. PEO represents an advanced anodizing process, whose application to the metallic materials results in the formation of ceramic-like oxide layers on their surfaces. The coating is produced on the surface as a result of short micro-discharges at high voltages in media of low-concentrated environmentally friendly electrolytes [1-4]. The PEO layers are usually hard and demonstrate strong adhesion to the substrate. Applications of PEO surfaces range from classical wear and corrosion protection to novel “smart” self-healing coatings, degradable biocompatible coatings with possible drug release *on demand*, or photoactive coatings for environmentally friendly wastewater cleaning [5-10]. In spite of many advantages, the PEO layers contain numerous open pores and cracks, which significantly compromise their barrier protective properties. Several methods were developed to overcome this obstacle, one of which is based on post-treatments including deposition of hydroxyapatite [11, 12], in-situ growth of layered double hydroxides (LDH) based nanocontainers [13-15], sol-gel coatings [16-18] or their combination [19]. Such

treatments lead not only to sealing of the PEO layers, but also to the improvement of wear and corrosion protection properties of the entire coating.

The latest investigations demonstrated high potential of metal organic frameworks (MOFs) based films as conversion coatings. MOFs represent a class of porous coordination polymers with high regular porous networks, which are made of metal ions (or metal clusters) connected by organic linkers. The unique physical-chemical properties of MOFs, which include broad structural and chemical variability, allowed widespread applications for gas storage and separation, catalysis, sensing, and drug delivery [20-23]. Additionally, due to their exceptional structure properties, MOFs demonstrate a high affinity to interact with both inorganic and organic compounds. Thus, the formation of a wide range of hybrid and composite materials is possible, and, consequently, with further broadening of MOFs properties [24-28]. Recently, different types of MOFs, namely ZIF-8 [29], bio-MOF-1 [30], MIL-53(Al) [31], Zn-MOF [32] have been reported to exhibit superb corrosion protective properties for Al and Mg based alloys. Moreover, the group of Liu developed a technique for controllable recrystallization of layered double hydroxide (LDH) coatings grown on the surface of aluminium into ZIF-8 [29] or ZIF-8@LDH [33] composite films demonstrating outstanding anticorrosion properties.

In this work, we firstly report the formation of a new type of coating via controllable transformation of a PEO layer on Z1 zinc alloy into ZIF-8 MOF in the presence of 2-methylimidazole (2-HmIm) linkers. ZIF-8 is a metal organic framework with sodalite (SOD) zeolite like structure formed by Zn^{2+} ions, which are connected by organic ligands (imidazolate, 2-mIm^- ions) [21]. This MOF is thermally and chemically stable [34] and also demonstrates hydrophobic and water stable properties [35]. The ZIF-8@PEO coating is expected to possess exceptional physical-chemical properties, as it combines the features of both: PEO ceramic parental layer and formed ZIF-8 metal organic framework, which can significantly broaden the areas of their potential applications. This article focuses on the detailed characterization of the structure of new coating and aims to understand mechanism of the PEO-to-MOF rearrangement.

2. Materials and methods

2.1. Substrate

Zinc alloy sheets with 1 mm thickness (Z1, according to EN988, VMZinc) with a composition of [wt.%]: 99.95 % Zn, 0.02 % Pb, 0.003 % Cu, 0.002 % Cd, 0.001 % Sn were used. The sheets were cut to a size of 30 x 20 x 1 mm or 25 x 20 x 1 mm (for nano-focused synchrotron X-ray diffraction analysis). Specimens were ground with 2500 silicon carbide (SiC) paper and cleaned with water before PEO treatment.

2.2. Reagents

For the preparation of PEO coatings potassium hydroxide (KOH, >99%, Sigma-Aldrich Chemie GmbH), trisodium phosphate (Na_3PO_4, techn., Alfa Aesar), were used. As solvents deionized water and methanol (CH_3OH, Carl Roth, ≥99.9%) were applied. 2-methylimidazole (2-HmIm, $CH_3C_3H_2N_2H$, Acros Organics, 99%) was used as an organic linker for the ZIF-8 formation.

2.3. PEO preparation

PEO coatings were prepared on the surface of Z1 zinc substrate specimen with the size of 30 x 20 x 1 mm using a pulsed DC power supply under a voltage and current limits of 300 V and 2 A, respectively. A pulse ratio of t_{on}:t_{off} = 1 ms:9 ms was used. The aqueous electrolyte contained 2 g/L KOH and 10 g/L Na_3PO_4. The treatment was performed under continuous stirring at 20 ± 2°C maintained by a circulating external water cooling system. The obtained samples were washed with water and dried under air.

2.4. Synthesis of ZIF-8@PEO coatings

ZIF-8@PEO coatings were synthesized by vapour-solid transformation (VST) in autoclave under thermal conditions (Figure S-1). For that purpose, a certain amount of 2-methylimidazole (2-HmIm) organic linkers (25, 50 or 100 mg) was added into the 30 ml autoclave, after the PEO coated samples were vertically placed into the same. The treatment with linker vapour was performed at 140 °C for 5 – 60 h. Table S-1 represents the details of the treatment conditions. Then, the samples were activated at 100 °C for 3 h under vacuum in order to remove 2-HmIm from the pores of ZIF-8. The samples were named as Z-n, were Z means ZIF-8, and n corresponds the particular time of the thermal treatment applied.

In order to compare VST and solvothermal treatment, PEO coated samples were placed into 25 ml 0.25 M 2-HmIm methanol solution and treated at 140 °C for 40 h. The obtained samples were washed with methanol for several times and dried for 16 h under room conditions.

2.5. Characterisation

The phase composition of the PEO and ZIF-8@PEO coatings was analysed using X-ray diffraction (XRD, Bruker D8 Advance, Ni filtered Cu Kα radiation source). The measurements were carried out under following settings: a glancing angle of 3°, a scan range from 3 till 50°, a step size of 0.02°, a scan speed of 1 s per step.

Surface morphology and cross-sections of obtained samples were studied using Tescan Vega3 SB scanning electron microscope (SEM) equipped with an eumeX energy dispersive X-ray (EDS) spectrometer. Prior to cross-section analysis, samples were embedded in resin, polished using 500, 1200, 2500, and 4000 grit silicon carbide (SiC) paper and then washed with deionized water. Morphology of the samples was analysed in SE mode, while cross section views were observed in BSE UniVac mode. Pore size distribution and amount of surface defects were analysed based on the SEM images using ImageJ program.

Further studies of the surface morphology and roughness of the PEO and ZIF-8@PEO coatings were performed through a laser scanning confocal microscope (LSM 800, ZEISS).

A glow discharge optical emission spectroscopy (GDOES) depth profile analysis of the obtained coatings was performed using a HORIBA GD-Profiler 2 at an operating pressure of 650Pa and a power of 30 W using a 4 mm anode.

The phase distribution across the PEO and ZIF-8@PEO coatings was analysed at the Deutsches Elektronen-Synchrotron (DESY) using the nano-focus end-station of the beamline P03 at PETRA III storage ring[36]. The experimental set-up is described in detail in the reference [37]. Data acquisition was done using an Eiger 9 M detector with pixel size of 75 µm by 75 µm. The X-ray beam had an energy of 19.7 keV and was focused to a beam size of 1.5 µm by 1.5 µm. A mesh scan across the coating regions interface was carried out on an area of 80 × 80 µm: 40

steps perpendicularly to the interface with a 2 µm step size, and 20 steps parallel to the interface with a step size of 4 µm. The acquisition time for each step was 0.5 s. Azimuthal integration was performed using PyFai [38].

Two different methods were used for the mechanical analysis of the samples: scratch-testing and hardness measurements. In both cases, analyses were performed using a STEP-100 Anton-Paar. The testing was performed according to DIN EN ISO 1512-2 and DIN EN ISO 4623-1 for scratch and indentation testing, respectively. For the scratch testing a standard Rockwell indenter was moved over the sample surface with linearly increasing load between 0.03 and 20 N over a total distance of 3.5 mm. For each scratch, the critical load points with adhesion damage were determined optically with the included light microscope. The hardness testing of cross sections was implemented with a standard Vickers indenter. Before the testing, PEO and ZIF-8@PEO samples were embedded in resin, ground with 500, 1200, 2500, 4000 grit silicon carbide (SiC) paper, polished using diamond particles (4 µm) and rinsed with deionized water. The hardness of the cross sections was measured seven to eight times, depending on coating thickness. The measurement started first on the soft zinc substrate, that was measured twice, then the PEO coating with two or three indents depending on the coating thickness. The ZIF-8 phase was analysed after that with one indent and ending on the soft resin with two measurements as well. The distance between each indent in zinc substrate was kept at 20 µm in order to avoid overlapping, the distance in coatings was kept at 10 µm and the applied force was 80 mN. This ensures enough distance between the indents to be seen as separate. Because of the low visibility of the indents on the coating, an optical analysis according to the standard was not feasible, so the hardness was calculated via measurement of penetration depth for all indents, in order to ensure comparability.The hardness (H_{IT}) was calculated in agreement with the ref. [39] using the equations 1-3:

$$H_{IT} = \frac{F_m}{A_p} \quad ,(1);$$

$$A_p = C_0 h_c^2 + C_1 h_c + C_2 h_c^{\frac{1}{2}} + C_3 h_c^{\frac{1}{4}} \quad \ldots, (2);$$

$$h_c = h_t - \varepsilon \frac{F_m}{S} \quad , (3),$$

where F_m represents the applied force and h_t – the penetration depth, the values obtained experimentally, and A_p is projected area of contact, h_c is the contact depth. The value of ε is a constant depending on the shape of the indenter, here 24.5 for a Vickers indenter, and C_x values are calibrated constants from the instrument.

3. Results and discussion

3.1. Properties of parent PEO coating

In accordance with our previous investigations, for the controllable PEO-to-ZIF-8 recrystallization, a PEO coating was selected that was mainly composed of ZnO (XRD, Figure 1; Table S-2) [40, 41]. The SEM images demonstrate that the surface of obtained PEO coating contains a high amount of pores (Figure 2, a, b). The pore size varies from ~0.6 to ~ 60 µm, the majority of them had a size less than 1 µm (Table 1). The Figure 2, c presenting the PEO cross-section shows that the PEO thickness was irregular with values from around 5 to 50 µm. The elemental mappings of cross section confirms the homogeneous distribution of Zn, O and P elements through the PEO layer (SI, Figure S-2.1).

3.2. PEO-to-ZIF-8 rearrangement

As-synthesised PEO coatings were subjected to vapour-solid transformation (VST) with 2-methylimidazole as the organic linker at 140 °C in an autoclave. Under conditions applied, 2-HmIm changes in the state of matter from solid to gas phase and then reacts with PEO coating forming ZIF-8 phase on the surface and inside of the PEO pores. The VST type of treatment was chosen due to its advantages over to traditional solvothermal ways of MOF synthesis, since it allows to avoid possible metal corrosion and chemical contamination (e.g. by solvents) [42]. Moreover, the most frequently used solvent for ZIF-8 synthesis is methanol and its exclusion from the synthesis significantly improves the technology regarding costs and, especially, safety as methanol belongs to the compounds, which usage is strongly restricted by the REACH regulations. However, for comparison, the ZIF-8@PEO coating was also prepared under solvothermal conditions via treatment of PEO plates with 0.25 M 2-HmIm methanol solution. The solvothermal treatment demonstrated its ineffectiveness, as very low intensity signals of ZIF-8 can be found in the XRD patterns (SI, Figure S-3) after the treatment of the plate at 140 °C

for 40 h. It signifies the advantage of the VST technique for conversion of PEO samples into ZIF-8.

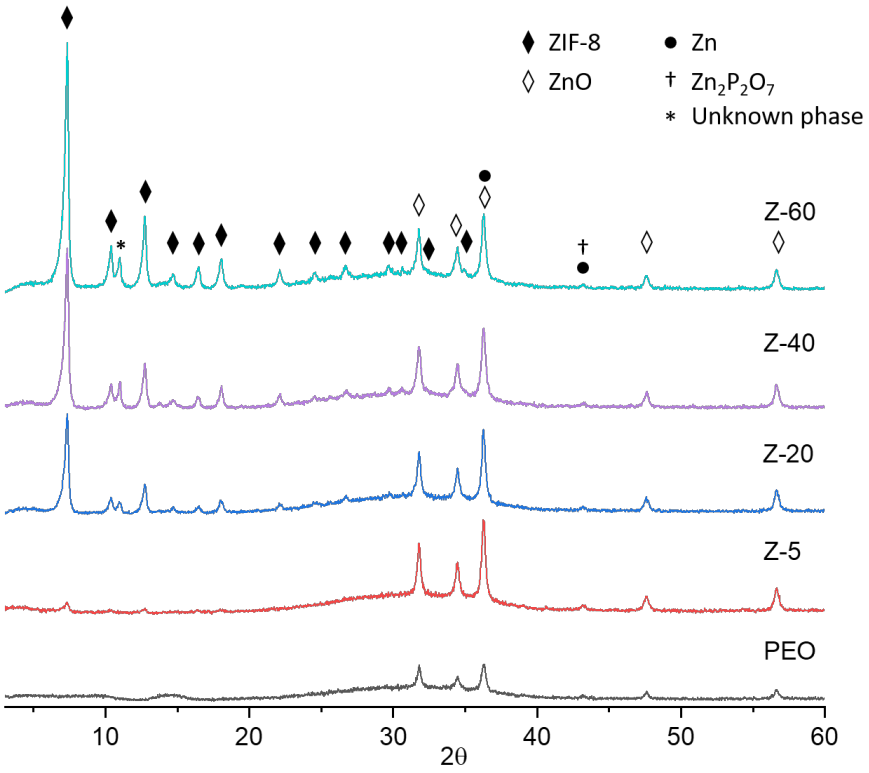

Figure 1. XRD patterns of initial Z1 alloy and the samples coated with PEO or ZIF-8@PEO and assignment of the diffraction peaks.

In order to follow the PEO-to-ZIF-8 conversion, we gradually increased the treatment time along with the amount of 2-methylimidazole linker (SI, Table S-1). The Figure 1 represents the XRD patterns of the prepared novel ZIF-8@PEO coating. The formation of MOF phase is already detected for Z-5 sample (5 h treatment in the presence of the lowest 2-HmIm amount). Experimental results demonstrate that the increase of the process time and 2-HmIm amount in the system are beneficial for improvement of the conversion rates of PEO layers into MOF nanocontainer. The intensities of the reflections corresponding to ZIF-8 phase gradually increase from samples Z-5 to Z-60. It indicates the presence of a high amount of the MOF phase in the coatings, especially after 60 h of the treatment (Z-60 specimen). However, a complete recrystallization of the PEO layer was not achieved even after 60 h of VST, as the reflections

corresponding to ZnO and $Zn_2P_2O_7$ phases are still visible in the XRD patterns. These data correlate with the chemical composition of ZIF-8@PEO specimens presented in the table S-2 showing the increased amount of C and N in Z-60 (elements deriving from organic linkers) and the presence of P and O (elements form PEO layer).

3.3. Analysis of elements distribution in ZIF-8@PEO coatings

Glow discharge optical emission spectroscopy (GDOES) depth profile analysis was performed to follow the elemental distribution in the course of the PEO-to-ZIF-8 conversion (Figure 3). GDOES was used as qualitative analysis allowing to evaluate the distribution of elements with depth from the surface. The coating thicknesses can be also estimated based on the change of the elemental profiles. Thus, while Z-5 and Z-20 possess a thickness similar to the initial PEO coating, the values for ZIF-8@PEO films obtained after 40 and 60 h are increased, which can be associated with formation of the MOF phase on the PEO surface.

Analysis of the depth profile for parent PEO sample (Figure 3, a) clearly indicates the presence of two regions. The regions are marked by a vertical broken lines for better visibility. The first region, where the level of the intensities of Zn, P and O signals exhibit plateaus, corresponds to the PEO layer (region II). After the PEO coating reaches the zinc substrate (region I), the intensity of zinc signal starts to increase along with a decreasing intensity of O and P signals down to the background level.

For the samples having experienced the VST treatment (Figure 3, b-e), an extra layer (region III) gets visible in the data, which is characterized by a significant amount of carbon, nitrogen and hydrogen, whose presence is negligible small (mainly adsorption from air) in the PEO coated zinc substrate. Increase in the intensities of C, N and H signals can be explained by the presence of 2-methylimidazolate ions forming the framework of ZIF-8. Increasing of the reaction time from 5 to 60 h and amount of treating 2-methylimidazole from 25 to 100 mg result in a significant growth of ZIF-8 layer thickness (Figure 3, c-e)) with respective sputtering times of 8, 24, 48 and 64 s for Z-5, Z-20, Z-40 and Z-60 respectively. Moreover, in contrast to Z-5, where profile of C is represented by a single signal, in the case of Z-20, Z-40 and Z-60, the signal of carbon is characterised by doublet. It can be speculated, that the presence of such a doublet

is related to the multilayered crystallization of ZIF-8 crystals on the PEO surface for these samples. The “ZIF-8 region” on the samples surface is directly followed by a standard plateau of Zn, P and O elements representing the PEO coating, whose thicknesses significantly decreases from the initial PEO sample to the Z-60 specimens. (Figure 3, b-e). It should be noticed that the intensities of C, N and H signals dramatically decreases after the reaching of “PEO region” in case of Z-5 indicating the presence of ZIF-8 phase only on the external surface of the coating. In contrast, for Z-20, Z-40 and Z-60, profiles of these elements are found also in the “PEO region”, which is related to the penetration of ZIF-8 phase into the original PEO layer especially deep for Z-40 and Z-60.

3.4. Surface morphology of the novel coatings

Similarly to the results of XRD and GDOES, the SEM analysis also confirms the formation of the MOF phase already at the early stages of the treatment (Figure 2). After 5 h of the VST, first tiny crystals with rhombic dodecahedron morphology, which is typical for ZIF-8, are located on the surface of the PEO coating (Figure 2, e). The further progress of the process led to the enlargement of the MOF crystals. In contrast to Z-5, containing crystals with a size of around 1 µm, for Z-20, the ZIF-8 crystals were enlarged up to 3-4 µm. Surprisingly, the increase of the treatment time to 40 h and the amount of 2-HmIm to 100 mg do not influence the crystal size. The Z-40 sample possesses a similar crystal size to Z-20. In turn, the long-term treatment (Z-60 sample: 60 h, 100 mg 2-HmIm) led to further growth of MOF crystals with preservation of their morphology. The crystals size reached a maximum value of ~ 8 µm.

3.5. Evolution of surface porosity in the course of PEO to ZIF-8 rearrangement

The growth of ZIF-8 crystals on the PEO surface was accompanied by the change of the surface porosity in the samples. For the treatment for 5 h using the lowest amount of the organic linker, numerous new pores and defects were formed. The quantitative analysis of pore distribution (Table 1) demonstrate, that, while the numbers of large pores (> 10 µm) are comparable for PEO and Z-5 specimens (60 ± 3 and 67 ± 8, respectively), the amount of small (< 1µm) and medium (between 1 and 10 µm) sized pores significantly rises. For the small sized pores numbers increases from 3131 ± 338 to 6029 ± 1436, and medium from 1566 ± 247 to

2274 ± 249 for PEO and Z-5 samples, respectively. This observation can be explained by the transformation of the PEO phase stimulated by 2-HmIm. However, based on the cross section (Figure 2, f), the PEO layer remains compact and significant dissolution across the thickness is not detected in the course of VSP for Z-5. This observation indicates that new pores were formed mainly on the upper part of the PEO layer, but not inner part was involved. In order to follow how the coating defects are healed during the PEO-to-MOF transformation, the percentage of defected surface area was estimated on the surface. While this value is 15.2 ± 1.2 % in the case of the parent PEO coating, for Z-5 the value increases to 16.0 ± 0.6 %. During the VSP treatment, a partial pore sealing (7.1 ± 0.9 %) could be seen, which is related to the homogeneous coating of the PEO surface by ZIF-8 crystals in the Z-20 specimen. However, in contrast to the results of the GDOES showing that the ZIF-8 phase penetrates into the PEO layer in Z-20 (Figure 3, c), the MOF phase was grown mainly on the external PEO surface based on cross section analysis (Figure 2, f), and only few areas with ZIF-8 crystals were found insight the PEO layer (SI, Figure S-2-3). The maximum sealing of the PEO pores and defects was achieved for the Z-40 sample. Only 4.4 ± 1.0 % of surface area could be identified as an open pore structure, as well as this sample demonstrates the lowest number of pores (3976 ± 769 in total). The cross sectional analysis confirms the presence of two layers: 1) outer MOF and 2) inner PEO, similarly to Z-20. However, in contrast to Z-20, the MOF phase in Z-40 is ubiquitously detectable inside the PEO pores. This observation also correlates with the EDX analysis of cross sections (Figures S-2). The mappings for Z-40 reveal the internal areas with low concentration of phosphorus and oxygen along with high concentration of zinc atoms, which can be associated with ZIF-8 phase formation (Figures S-2.4). Finally, after the long-term treatment (60 h, Z-60 sample) high amounts of ZIF-8 are located in both external and internal PEO surfaces. However, such a long high-temperature treatment results in the formation of cracks on the surface, i.e. leading to the generation of new defects, which are characterised by an estimated value of 4.5 ± 0.5 %.

Table 1. Quantitative analysis of pore size distribution of PEO and Z-N samples

Sample	< 1 µm	1 < x < 10 µm	> 10 µm	Total amount
PEO	3131 ± 338	1566 ± 247	60 ± 3	4757 ± 370
Z-5	6029 ± 1436	2274 ± 249	67 ± 8	8370 ± 1608
Z-20	2798 ± 490	1320 ± 257	27 ± 14	4145 ± 729

Z-40	2625 ± 672	1344 ± 201	7 ± 5	3976 ± 769
Z-60	2911 ± 446	1425 ± 216	13 ± 5	4349 ± 606

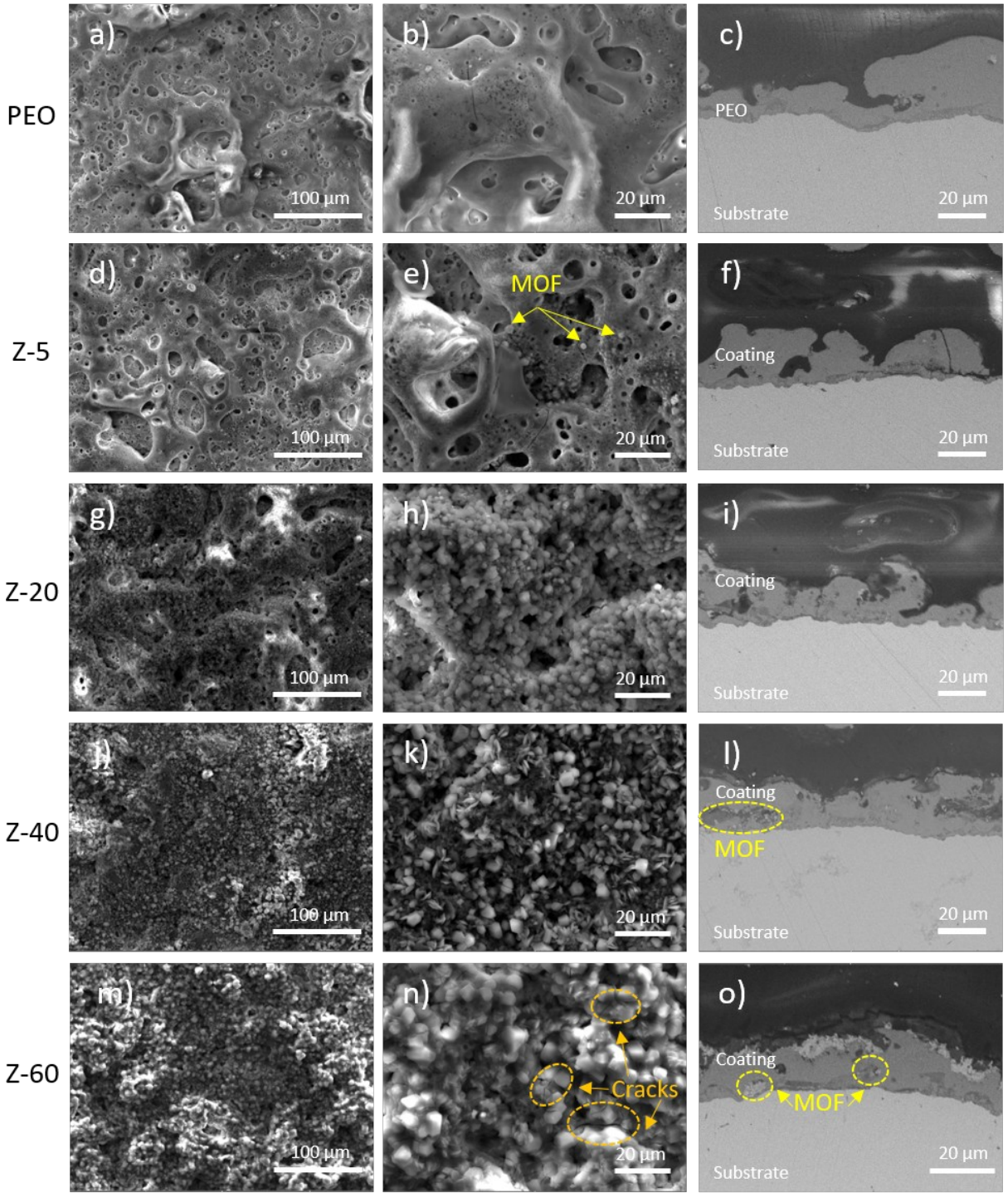

Figure 2. SEM images of surface morphology and corresponding cross-sections of Z-1 covered with a)-c) PEO, d)-f) Z-5, g)-i) Z-20, j)-l) Z-40 and m)-o) Z-60. Surface morphology was analyzed in SE mode, the cross sections were studied in BSE UniVac mode.

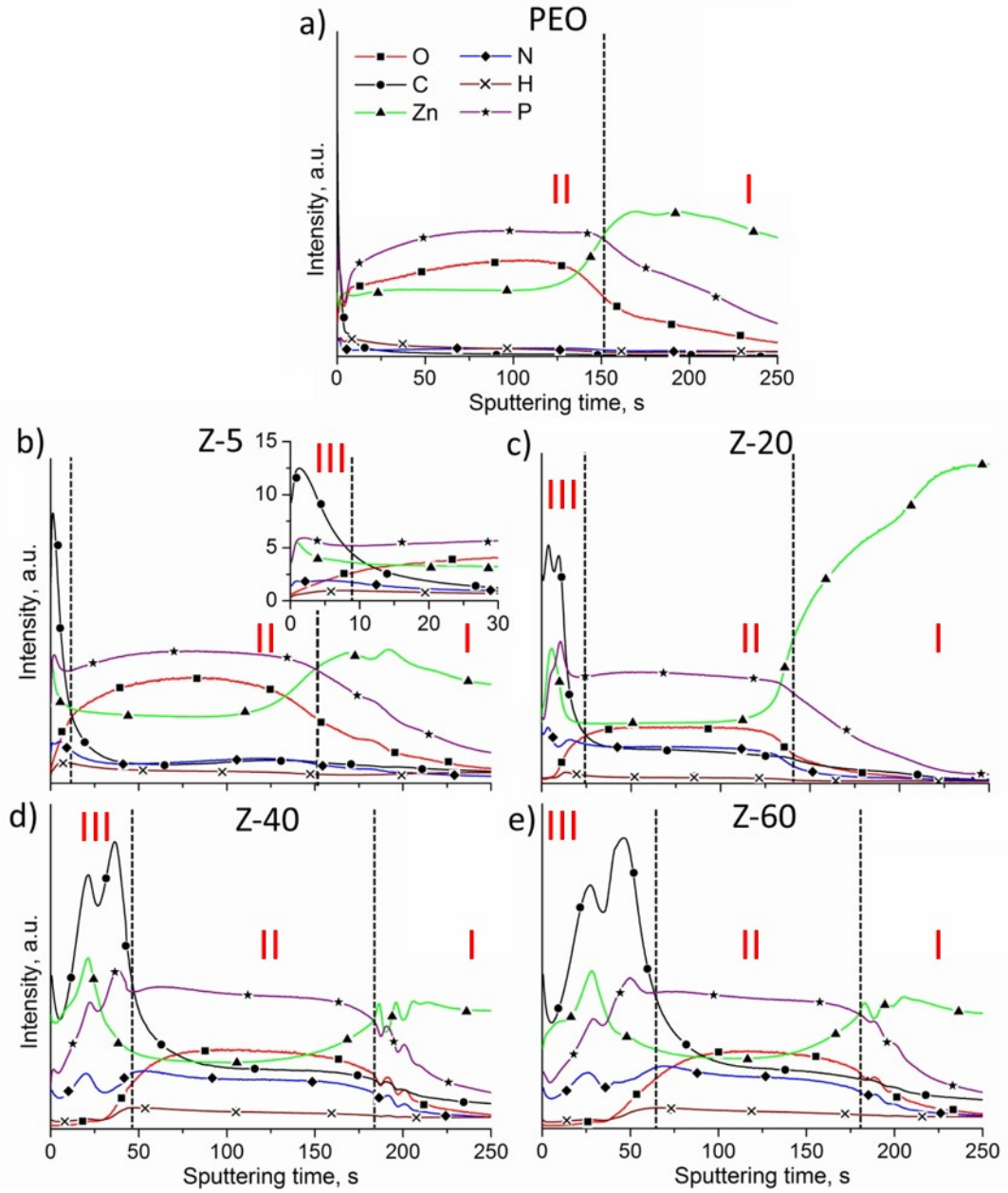

Figure 3. Qualitative glow discharge optical emission spectrometry (GDOES) depth profiles for Z1 alloy coated with a) PEO, b) Z-5, c) Z-20, d) Z-40 and e) Z-60. Insert in Figure 3, b clearly shows presence of thin ZIF-8 region in Z-5 sample. The vertical broken lines indicate the transition from one layer to the other: I) substrate, II) “PEO layer region” and III) “ZIF-8 region”.

3.6. Phase distribution across the thickness of ZIF-8@PEO coatings

In order to understand the phase distribution across the thickness of the coating a nano-focused synchrotron X-ray diffraction analysis was performed. Figures S-4 represents selected high-resolution localized XRD patterns of the PEO coatings and samples subjected to VST for 5,

20 and 60 h. The phases present in the coatings are Zn, ZnO, $Zn_2P_2O_7$ and ZIF-8 (for samples after VST), which is in agreement with the XRD data presented in Figure 1. For the detail characterisation of the phase distribution within the PEO-to-ZIF-8 conversion layer, the distribution of the local intensities of the main phases, namely, ZnO (100 reflection) and ZIF-8 (222 reflection) was analysed. Based on the data obtained, the two-dimensional maps representing the spatial distribution of the phases across the coating thickness were created.

The thickness of the obtained coatings varies from approximately 30 to 50 µm. These results partially correlate with the cross-sections, demonstrating the change of the thickness in the broader range, namely from 5 till 50 µm, as for the parental PEO coating, as for ZIF-8@PEO layers. Such a difference is related to the differences in experimental settings. As in the case of two-dimensional maps, the analysing region was limited by the area of 80 µm x 80 µm, the cross sections were studied through the whole specimen lengths.

The main phase, which is distributed within initial PEO coating, is zinc oxide, which correlates with XRD data presented in the Figure 1. Similarly to PEO, ZnO was spread through the entire thickness of the coatings obtained after 5 and 20 h of VST. Oppositely, on the 2D mapping for Z-60 the areas with different intensities of ZnO can be clearly seen indicating an inhomogeneity within the layer. This effect can be related to the partial transformation of ZnO phase into the MOF. Analysis of the distribution of ZIF-8 (Figure 4, d, f, h) confirms that the MOF is formed on the surface of PEO even after 5h of the treatment, which is in agreements with cross sections and SEM. For Z-5 and Z-20 samples, ZIF-8 was located mostly on the upper part of the coating, while for the sample treated for 60 h, the phase is distributed through the entire coating with the highest intensities in the inferior area of the film (Figure 4, h). This enhanced intensity of the MOF can be associated with the sealing of the PEO defects by the formed MOF phase, similarly as it was observed in the SEM micrographs (Figure 2, o).

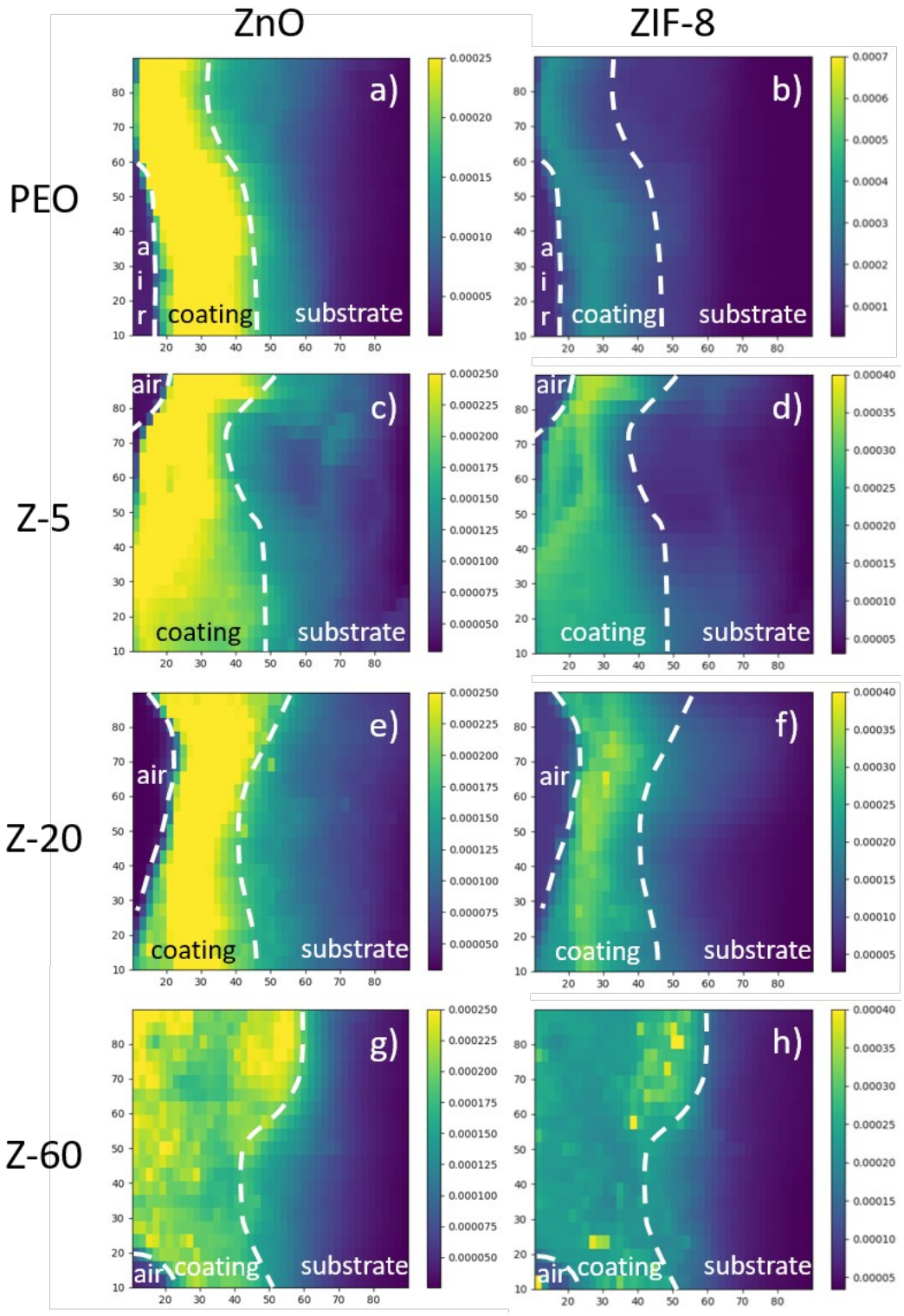

Figure 4. 2D maps of phase distribution across coating thickness on PEO: a) ZnO, b) ZIF-8; on Z-5: c) ZnO, d) ZIF-8; on Z-20: e) ZnO, f) ZIF-8; and Z-60: g) ZnO, h) ZIF-8.

3.7. Roughness of ZIF-8@PEO coatings

Analysis of the surface roughness of prepared samples studied by LSM (Figure 5) showed that vapour-solid transformation of PEO coatings results in the surface smoothing. The value of surface roughness are comparable for the parent PEO and Z-5, 7.64±0.89 µm and 7.54±0.33 µm respectively, than gradually decreased to the value of 4.22 ± 0.70 µm for Z-60. In the case of parent PEO and Z-5, the high values of roughness are related to the presence of numerous surface pores with different size and deepness. The following smoothing of the surface for Z-20, Z-40 and Z-60 was observed as a result of the sealing of these pores by ZIF-8 crystals. These results correlate with the SEM data, however, it should be noticed, that cracks of the crystals occurring during long-term treatment (60 h), do not led to the increase of the surface roughness, and Z-60 sample possesses the most uniform and flat surface among all samples.

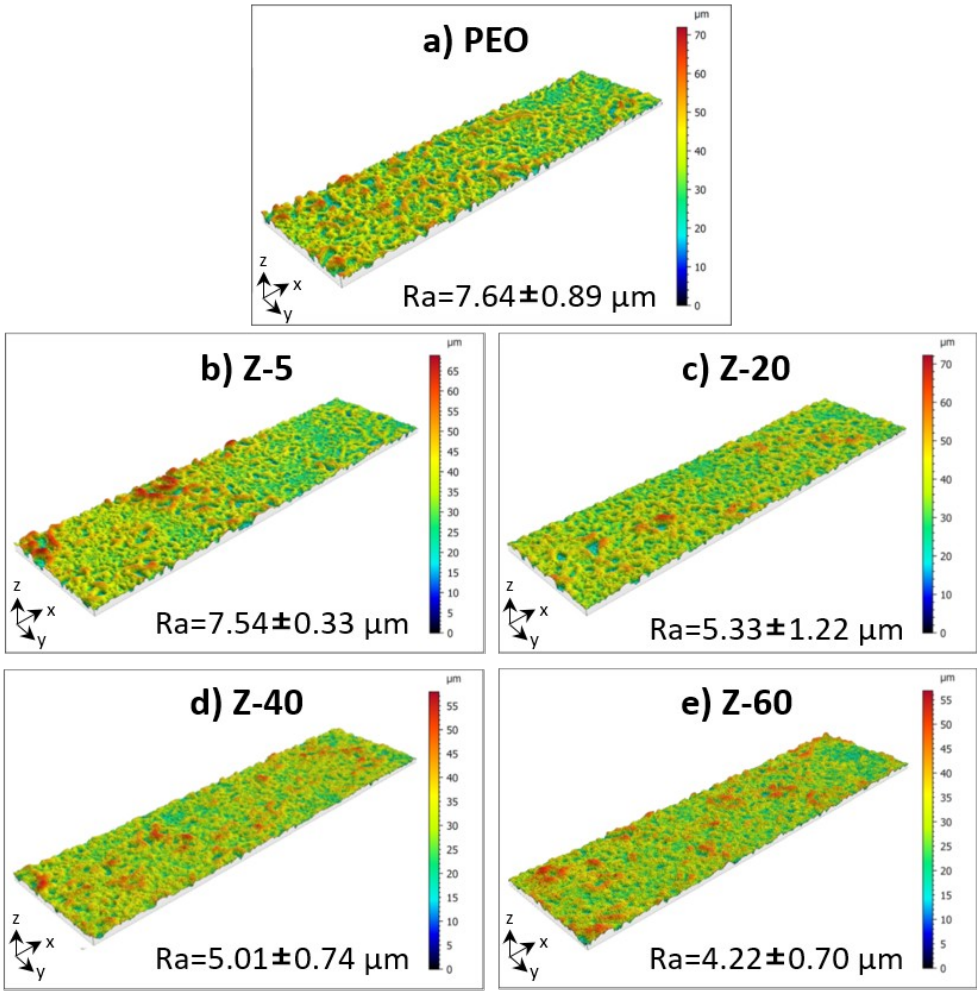

Figure 5. Surface profiling of initial PEO coating and after the treatment with 2-HmIm. Ra represents corresponding values of the roughness for each of the sample.

3.8. Evolution of mechanical properties

The evolution of the mechanical properties in course of the recrystallization of ZnO based PEO into ZIF-8 was studied by scratch-testing (Table 2, SI, Figure S-5) and hardness measurement of the cross sections (SI, Figures S-6). The adhesion damage of the surface decreased with higher degree of PEO to ZIF-8 transformation. The values of the adhesion gradually decreased from 3700 ± 742 mN for parent PEO till 3127 ± 342 mN for Z-60.

The hardness testing was evaluated for the cross sections of the specimens. Such a way of analysis allows to follow the hardness properties of each of the component of the coating and understand how the degree of PEO-to-ZIF-8 transformation affects the values. For all specimens, PEO and ZIF-8 modified PEO coatings, the presence of two regions is clearly visible: the region of the zinc substrate and “PEO-region”. Rearrangement does not involve the substrate and its region is characterised by the hardness of 55-75 HV for all samples. In contrast, the hardness in „PEO region“ varies in the range from 200 till 320 HV. Such a variation is associate with dissolution of PEO phase under treatment conditions and its following transformation into softer ZIF-8 phase. Analysis of cross sections of the Z-20, Z-40 and Z-60 samples showed also the presence of the soft “ZIF-8 region” with the hardness of 40-55 HV.

Table 2. Adhesion damage of the samples

	PEO	Z-5	Z-20	Z-40	Z-60
Adhesion damage, mN	3700 ± 742	3569 ± 725	3328 ± 407	3402 ± 1510	3127 ± 342

3.9. Mechanism of PEO-to-ZIF-8 transformation

Summarising the results discussed previously, the following mechanism of PEO-to-ZIF-8 transformation can be proposed (Figure 6). 2-Methylimidazole sublimates under the treatment conditions and leads to partial transformation of the PEO layer. This process is accompanied by the formation of additional pores and by the enlargement of the already existing in the layer. In turn, zinc ions released from PEO reacts with the organic ligand forming first tiny ZIF-8 crystals on the outer surface of the coating (stage 1). Prolongation of the process leads to the crystals‘

enlargement, which starts to seal pores on the PEO surface (stage 2). Then ZIF-8 crystals begin to deposit not only on the external surface, but also on the internal surfaces of PEO coating leading to effective sealing of surface defects. In this context, presence of numerous cracks and pores in the structure of PEO can be considered as an advantage, since they facilitate transport of 2-HmIm to inner interfaces of the coating, and thus allowing MOF formation through the entire layer. It should be noticed that along with the increase of the number of MOF crystals, their size remain constant during this stage (stage 3). It can be related to the fact that the transformation insight the layer runs faster due to high availability of Zn ions. In turn, it leads to depletion of 2-mlm at the top of the PEO layer and thus to retard of ZIF-8 crystals growth. After the maximum sealing of interface and, thus, a blocking for diffusion of 2-mlm insight to the layer, the concentration of 2-mlm increase again leading to further growth of the ZIF-8 crystals (from 3-4 μm to 8 μm) (stage 4). However, this process is accompanied with the cracking of ZIF-8 crystals, i.e. formation of new defects on the surface, which can be related to stress in the layer appearing due to the growth of the crystals on the PEO surface in all directions. These results demonstrate that the optimum formation of ZIF-8@PEO film happening at specific reaction times (40 h) and appropriate amounts of the ligand (which depends on the size of PEO coated plates, here 100 mg). Moreover, by varying the conditions of the VST process, it seems possible to control the formation of the coatings with desired PEO-to-ZIF-8 ratio, different ZIF-8 loading and distributions in the PEO. Another feature of the process is its inability to achieve a complete PEO-to-ZIF-8 conversion. It can be speculated that the large ZIF-8 crystals, which are formed on the PEO surface and after seal the defects and pores, could block further access of 2-HmIm to the PEO surface thereby terminating the process of the vapour-solid transformation.

4. Conclusions

For the first time we have reported the formation of novel ZIF-8@PEO coatings via vapour-state transformation of PEO type coating obtained on the surface of zinc substrate using 2-methylimidazole as organic linker. The process takes place via a multi-step mechanism, starting with partial PEO dissolution stimulated by 2-HmIm, which is followed by gradual crystallisation of ZIF-8 on external and internal coating surfaces. It results in the sealing of the PEO defects, which along with loading of ZIF-8 crystals can be controlled by varying the

treatment conditions. Due to the combination of the features of PEO layers, as high adhesion to the surface and ZIF-8, the novel coating is assumed to exhibit unique physical-chemical properties, like enhanced corrosion resistance in combination with Lewis acidity and shape selectivity etc. They make the obtained materials potential candidates for future application in corrosion protection, and for photo- and heterogeneous catalysis.

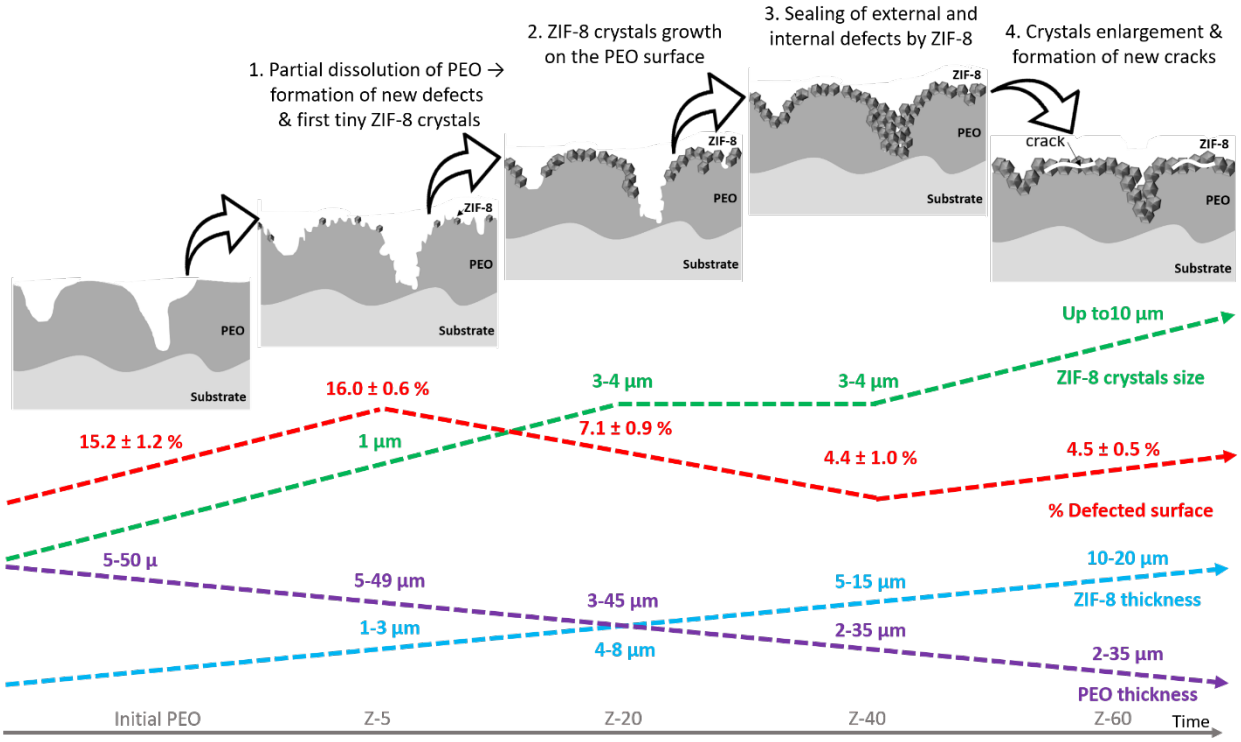

Figure 6. Schematic representation of the mechanism of PEO-to ZIF-8 conversion. Green arrow shows the tendency in the change of ZIF-8 crystals size, green numbers correspond to approximate crystals sizes for Z-5 – Z-60 samples. Red arrow represents the tendency in the sealing of the surface defects in the coatings. Red numbers are the estimated percentage of the defected surface calculated based on the SEM images. Blue and violet arrows exhibit the tendency in the change of the thicknesses of ZIF-8 layer on the surface and PEO layer, respectively. The blue and violet numbers correspond to the maximum possible thicknesses for ZIF-8 and PEO layers, calculated from SEM data.

Acknowledgment

Dr. Valeryia Kasneryk is grateful for financial support from Alexander von Humboldt Foundation. The authors thank PETRA III (Hamburg, Germany) for accepting and granting the proposal I-20211343 (P.03 end-station) for localized phase composition analysis of the samples. The

authors also thank Dr. Anton Davydok for the experimental support during DESY beamline experiments and Mr. Volker Heitmann, Mr. Ulrich Burmester for technical support.

References

[1] A.L. Yerokhin, X. Nie, A. Leyland, A. Matthews, S.J. Dowey, Plasma electrolysis for surface engineering, Surface and Coatings Technology, 122 (1999) 73-93.
[2] F. Simchen, M. Sieber, A. Kopp, T. Lampke, Introduction to Plasma Electrolytic Oxidation—An Overview of the Process and Applications, Coatings, 10 (2020) 628.
[3] S. Sikdar, P.V. Menezes, R. Maccione, T. Jacob, P.L. Menezes, Plasma Electrolytic Oxidation (PEO) Process—Processing, Properties, and Applications, Nanomaterials, 11 (2021).
[4] T.W. Clyne, S.C. Troughton, A review of recent work on discharge characteristics during plasma electrolytic oxidation of various metals, International Materials Reviews, 64 (2019) 127-162.
[5] S. Ignjatović, C. Blawert, M. Serdechnova, S. Karpushenkov, M. Damjanović, P. Karlova, D.C.F. Wieland, M. Starykevich, S. Stojanović, L. Damjanović-Vasilić, M.L. Zheludkevich, Formation of multi-functional TiO2 surfaces on AA2024 alloy using plasma electrolytic oxidation, Applied Surface Science, 544 (2021) 148875.
[6] M. Aliofkhazraei, D.D. Macdonald, E. Matykina, E.V. Parfenov, V.S. Egorkin, J.A. Curran, S.C. Troughton, S.L. Sinebryukhov, S.V. Gnedenkov, T. Lampke, F. Simchen, H.F. Nabavi, Review of plasma electrolytic oxidation of titanium substrates: Mechanism, properties, applications and limitations, Applied Surface Science Advances, 5 (2021) 100121.
[7] K. Babaei, A. Fattah-alhosseini, R. Chaharmahali, A review on plasma electrolytic oxidation (PEO) of niobium: Mechanism, properties and applications, Surfaces and Interfaces, 21 (2020) 100719.
[8] K.V. Nadaraia, S.N. Suchkov, I.M. Imshinetskiy, D.V. Mashtalyar, S.L. Sinebrykhov, S.V. Gnedenkov, Some new aspects of the study of dependence of properties of PEO coatings on the parameters of current in potentiodynamic mode, Surface and Coatings Technology, 426 (2021) 127744.
[9] K. Yu, P. Li, Q. Han, Q. Wang, S.A. Karpushenkov, X. Lu, O.V. Ignatenko, Investigation of biodegradability, cytocompatibility and antibacterial property of plasma electrolytic oxidation coating on Mg, Surfaces and Interfaces, 30 (2022) 101840.
[10] D.V. Mashtalyar, K.V. Nadaraia, N.G. Plekhova, I.M. Imshinetskiy, M.A. Piatkova, A.I. Pleshkova, S.E. Kislova, S.L. Sinebryukhov, S.V. Gnedenkov, Antibacterial Ca/P-coatings formed on Mg alloy using plasma electrolytic oxidation and antibiotic impregnation, Materials Letters, 317 (2022) 132099.
[11] Q. Zhao, X. Guo, X. Dang, J. Hao, J. Lai, K. Wang, Preparation and properties of composite MAO/ECD coatings on magnesium alloy, Colloids and Surfaces B: Biointerfaces, 102 (2013) 321-326.
[12] J.H. Gao, S.K. Guan, J. Chen, L.G. Wang, S.J. Zhu, J.H. Hu, Z.W. Ren, Fabrication and characterization of rod-like nano-hydroxyapatite on MAO coating supported on Mg–Zn–Ca alloy, Applied Surface Science, 257 (2011) 2231-2237.
[13] M. Serdechnova, M. Mohedano, A.C. Bouali, D. Hoche, B. Kuznetsov, S. Karpushenkov, C. Blawert, M.L. Zheludkevich, Role of Phase Composition of PEO Coatings on AA2024 for In-Situ LDH Growth, Coatings, 7 (2017).
[14] Y. Li, X. Lu, M. Serdechnova, C. Blawert, M.L. Zheludkevich, K. Qian, T. Zhang, F. Wang, Incorporation of LDH nanocontainers into plasma electrolytic oxidation coatings on Mg alloy, Journal of Magnesium and Alloys, (2021).
[15] G. Zhang, L. Wu, M. Serdechnova, A. Tang, C. Wang, C. Blawert, F. Pan, M.L. Zheludkevich, In-situ LDHs growth on PEO coatings on AZ31 magnesium alloy for active protection: Roles of PEO composition and conversion solution, Journal of Magnesium and Alloys, (2021).

[16] L. Sopchenski, J. Robert, M. Touzin, A. Tricoteaux, M.-G. Olivier, Improvement of wear and corrosion protection of PEO on AA2024 via sol-gel sealing, Surface and Coatings Technology, 417 (2021) 127195.
[17] L. Pezzato, M. Rigon, A. Martucci, K. Brunelli, M. Dabalà, Plasma Electrolytic Oxidation (PEO) as pre-treatment for sol-gel coating on aluminum and magnesium alloys, Surface and Coatings Technology, 366 (2019) 114-123.
[18] R.d.O. Silva, A.C. Silvino, J.M. Ribeiro, K. Dahmouche, Novel sol–gel derived PLA-siloxane-PEO nanocomposite with enhanced thermal properties and hydrolytic stability, Journal of Sol-Gel Science and Technology, 99 (2021) 512-526.
[19] A.C. Bouali, E.A. Straumal, M. Serdechnova, D.C.F. Wielan, M. Starykevich, C. Blawert, J.U. Hammel, S.A. Lermontov, M.G.S. Ferreira, M.L. Zheludkevich, Layered double hydroxide based active corrosion protective sealing of plasma electrolytic oxidation/sol-gel composite coating on AA2024, Applied Surface Science, 494 (2019) 829-840.
[20] M. Opanasenko, Catalytic behavior of metal-organic frameworks and zeolites: Rationalization and comparative analysis, Catalysis Today, 243 (2015) 2-9.
[21] J. Zhang, Y. Tan, W.-J. Song, Zeolitic imidazolate frameworks for use in electrochemical and optical chemical sensing and biosensing: a review, Microchimica Acta, 187 (2020) 234.
[22] Q. Qian, P.A. Asinger, M.J. Lee, G. Han, K. Mizrahi Rodriguez, S. Lin, F.M. Benedetti, A.X. Wu, W.S. Chi, Z.P. Smith, MOF-Based Membranes for Gas Separations, Chemical Reviews, 120 (2020) 8161-8266.
[23] L. Wang, M. Zheng, Z. Xie, Nanoscale metal–organic frameworks for drug delivery: a conventional platform with new promise, Journal of Materials Chemistry B, 6 (2018) 707-717.
[24] Z. Wang, J. Huang, J. Mao, Q. Guo, Z. Chen, Y. Lai, Metal–organic frameworks and their derivatives with graphene composites: preparation and applications in electrocatalysis and photocatalysis, Journal of Materials Chemistry A, 8 (2020) 2934-2961.
[25] A. Amini, S. Kazemi, V. Safarifard, Metal-organic framework-based nanocomposites for sensing applications – A review, Polyhedron, 177 (2020) 114260.
[26] D. Giliopoulos, A. Zamboulis, D. Giannakoudakis, D. Bikiaris, K. Triantafyllidis, Polymer/Metal Organic Framework (MOF) Nanocomposites for Biomedical Applications, Molecules, 25 (2020) 185.
[27] Z. Zhang, Z. Cai, Z. Wang, Y. Peng, L. Xia, S. Ma, Z. Yin, Y. Huang, A Review on Metal–Organic Framework-Derived Porous Carbon-Based Novel Microwave Absorption Materials, Nano-Micro Letters, 13 (2021) 56.
[28] P. Rani, V. Kasneryk, M. Opanasenko, MOF-inorganic nanocomposites: Bridging a gap with inorganic materials, Applied Materials Today, (2021) 101283.
[29] M. Zhang, L. Ma, L.L. Wan, Y.W. Sun, Y. Liu, Insights into the Use of Metal-Organic Framework As High-Performance Anticorrosion Coatings, Acs Applied Materials & Interfaces, 10 (2018) 2259-2263.
[30] W. Liu, Z. Yan, Z. Zhang, Y. Zhang, G. Cai, Z. Li, Bioactive and anti-corrosive bio-MOF-1 coating on magnesium alloy for bone repair application, Journal of Alloys and Compounds, 788 (2019) 705-711.
[31] Y.J. Tarzanagh, D. Seifzadeh, Z. Rajabalizadeh, A. Habibi-Yangjeh, A. Khodayari, S. Sohrabnezhad, Sol-gel/MOF nanocomposite for effective protection of 2024 aluminum alloy against corrosion, Surface and Coatings Technology, 380 (2019) 125038.
[32] Y. Zhang, J. Wang, S. Zhao, M. Serdechnova, C. Blawert, H. Wang, M.L. Zheludkevich, F. Chen, Double-Ligand Strategy to Construct an Inhibitor-Loaded Zn-MOF and Its Corrosion Protection Ability for Aluminum Alloy 2A12, ACS Applied Materials & Interfaces, 13 (2021) 51685-51694.
[33] M. Zhang, Y. Liu, Enhancing the anti-corrosion performance of ZIF-8-based coatings via microstructural optimization, New Journal of Chemistry, 44 (2020) 2941-2946.
[34] K.S. Park, Z. Ni, A.P. Côté, J.Y. Choi, R. Huang, F.J. Uribe-Romo, H.K. Chae, M. O'Keeffe, O.M. Yaghi, Exceptional chemical and thermal stability of zeolitic imidazolate frameworks, Proceedings of the National Academy of Sciences, 103 (2006) 10186-10191.

[35] H. Zhang, M. Zhao, Y.S. Lin, Stability of ZIF-8 in water under ambient conditions, Microporous and Mesoporous Materials, 279 (2019) 201-210.
[36] C. Krywka, H. Neubauer, M. Priebe, T. Salditt, J. Keckes, A. Buffet, S.V. Roth, R. Doehrmann, M. Mueller, A two-dimensional waveguide beam for X-ray nanodiffraction, Journal of Applied Crystallography, 45 (2012) 85-92.
[37] T. Wu, C. Blawert, M. Serdechnova, P. Karlova, G. Dovzhenko, D.C.F. Wieland, M.L. Zheludkevich, PEO processing of AZ91Nd/Al2O3 MMC-the role of alumina fibers, Journal of Magnesium and Alloys, (2021).
[38] G. Ashiotis, A. Deschildre, Z. Nawaz, J.P. Wright, D. Karkoulis, F.E. Picca, J. Kieffer, The fast azimuthal integration Python library: pyFAI, Journal of Applied Crystallography, 48 (2015) 510-519.
[39] M. Griepentrog, C. Ullner, A. Dück, Instrumented indentation test for hardness and materials parameter from millinewtons to kilonewtons, 2002.
[40] M. Serdechnova, C. Blawert, S. Karpushenkov, L. Karpushenkava, T. Shulha, P. Karlova, R. Vasilić, S. Stojadinović, S. Stojanović, L. Damjanović-Vasilić, V. Heitmann, S.M. Rabchynski, M.L. Zheludkevich, Properties of ZnO/ZnAl2O4 composite PEO coatings on zinc alloy Z1, Surface and Coatings Technology, 410 (2021) 126948.
[41] C. Blawert, S.A. Karpushenkov, M. Serdechnova, L.S. Karpushenkava, M.L. Zheludkevich, Plasma electrolytic oxidation of zinc alloy in a phosphate-aluminate electrolyte, Applied Surface Science, 505 (2020) 144552.
[42] I. Stassen, M. Styles, G. Grenci, Hans V. Gorp, W. Vanderlinden, Steven D. Feyter, P. Falcaro, D.D. Vos, P. Vereecken, R. Ameloot, Chemical vapour deposition of zeolitic imidazolate framework thin films, Nature Materials, 15 (2016) 304-310.